THE JOURNAL OF PHYSICAL CHEMISTRY B

Article

pubs.acs.org/JPCB

# Influence of the Shape of Crowding Particles on the Structural Transitions in a Polymer

Alexander Kudlay,[†] Margaret S. Cheung,[‡] and D. Thirumalai*[,†,§]

[†]Biophysics Program, Institute for Physical Sciences and Technology, and [‡]Department of Physics, University of Houston, Houston, Texas 77204, United States

[§]Department of Chemistry and Biochemistry, University of Maryland, College Park, Maryland 20742, United States

**ABSTRACT:** We investigate the structural transitions in a polymer induced by spherical and nonspherical crowding particles over a wide range of conditions. The polymer conformations are specified by the radius of gyration and the quality of the solvent in the absence of crowding particles. In the presence of crowding particles, the structures are altered by the volume fraction, size, shape, and polydispersity of the crowders. We show that crowding induces an array of structural changes, ranging from helix, helical hairpin (HH), and multiple helix bundles (HBs), depending on the interplay of multiple length and energy scales including the solvent quality, length of the polymer, temperature, and the characteristics of the crowding agents. In nearly good solvents, the polymer undergoes coil−helix transition in accord with the predictions based on the entropic stabilization mechanism. Higher-order (HH and HB) structures are obtained in poor or moderately poor solvents. In a binary mixture of spherical crowders, the effect of the two components is largely additive with the polymer undergoing greater compaction at higher volume fraction. In contrast to spherical crowders, spherocylinder-like crowders have a dramatically different effect on the diagram of states of the polymer. In the presence of spherocylinders, the polymer prefers to form a nearly ideal helix, especially at low temperatures and high aspect ratios of the crowders, at volume fractions that are not large enough for nematic order. Surprisingly, there is a complete absence of HH and HB in the range of conditions explored here. The dominant formation of spherocylinder-induced helix formation is due to the tendency of the spherocylinders and the polymer to align along the director formed by an increase in nematic order only in the vicinity of the polymer. Our study, which has produced several testable predictions, shows that only by probing the effects of crowding on a polymer (or a protein and RNA) over a wide range of conditions can the diagram of states be quantitatively described.

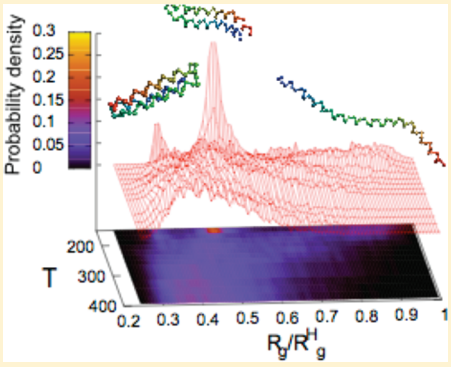


## INTRODUCTION

There is considerable interest in exploring the effects of macromolecular crowding on the folding of proteins[1−7] and RNA[8−10] because they provide a caricature of self-assembly in the more complex cellular environment. In vitro experimental[11−13] and theoretical studies cited above and others discussed in the excellent reviews[1,2,14] capture the ever-present effects of excluded volume interactions on the stability and folding kinetics of proteins and RNA. To understand the enhanced stabilities of proteins, it suffices to realize[6] that due to volume excluded by the crowding particles the polypeptide chain cannot explore only a restricted subset of all conformational space. On the basis of this observation, the enhanced stabilities of proteins have been determined in important studies[7] based on estimates of volume accessed by the protein, specified by the radius of gyration of a given conformation, in the presence of a crowding particle of appropriate shape. The observed crowding-induced enhancement in the stabilities of the folded states of proteins in experiments[3,13] is in accord with the predictions of the entropic stabilization mechanism (ESM). According to the ESM,[4,15] crowding decreases the entropy of both the folded and the unfolded states. However, the decrease in entropy of the unfolded states is considerably higher than the folded state, resulting in the increased stability of the native state. The ESM when used with polymer concepts yields quantitative predictions on the extent of increase of the melting temperature involving only the statistics of the unfolded conformations.[4] These predictions have been quantitatively validated in experiments.[3,13,16] Although qualitatively similar to other treatments,[7] the ESM[4] accounts for multiparticle fluctuations of the crowding agents and the conformations of proteins on equal footing. In other words, these fluctuations have been treated self-consistently, which makes deriving analytic expressions almost impossible, in contrast to approximate treatments.[7] The lack of self-consistency gives rise to differences in stability predictions between approximate treatments and simulations, which support the ESM (see

**Special Issue:** Macromolecular Systems Understood through Multiscale and Enhanced Sampling Techniques

**Received:** December 28, 2011
**Revised:** May 18, 2012
**Published:** May 22, 2012

especially Table S4 in[17] which compares the results of ESM and more approximate treatments).

With the exception of a few recent studies,[7,18,19] almost all of the theoretical studies have modeled crowding agents as monodisperse spherical particles. Such a description may be adequate in rationalizing experimental results that are obtained using Ficoll, polyethylene glycol, and dextran as crowding agents. It should be emphasized that to obtain quantitative agreement with experiments it may be necessary to consider not only the shapes of crowding particles but also nonspecific attractive interactions between crowding agents and proteins.[20,21] Indeed, as pointed out in ref 18, the nonspherical shapes of macromolecules as well as polydispersity due to variations in composition and sizes of macromolecules in cells could have a dramatic effect on protein stability. Similarly, the shapes of crowding particles can not only influence protein stability but also have a profound influence on protein association[2] and oligomer formation in an amyloidogenic peptide.[19] Recently, we[22] showed that spherical crowding agents induce a series of structural transitions, such as helical hairpin (HH) and multiple helix bundles (HBs), in a homopolymer depending on the length, $N$, of the chain, volume fraction, $\phi_c$, and the quality of the solvent. Although the homopolymer may not be of direct relevance to proteins, it constitutes a well-defined system for which precise computations can be performed. More importantly, these systems are relevant in understanding crowding-induced structure formation in synthetic polymers[23] for which external conditions such as solvent quality can be varied to a greater extent than can be achieved for biopolymers.

Understanding the effect of macromolecular crowding on polymers is a classic problem involving an interplay of several length scales. Minimally, the system of interest is a ternary system consisting of protein, solvent, and crowding particles. The size of the solvent is about 0.3 nm, whereas the radius of gyration, $R_g$, of the polymer can be controlled by $N$ and the solvent quality can be greater than several nanometers. The crowding particles considered here are either spheres with radius $r_c$ or rodlike with length $L$ and radius $r_c$. In addition to these length scales, crowding-induced structural changes in the polymer are also influenced by the energy scales associated with the polymer. Assuming that the effect of the solvent can be integrated out, we still have a system with two or more length and energy scales. Describing the interplay between these energy and length scales requires models for which precise simulations can be carried out. Here, we explore the interplay between them in influencing the structural transitions in a homopolymer using a coarse-grained (CG) description of the polymer as well as the crowding particles. We predict a remarkably rich series of crowding-induced ordered structure formation ranging from helical hairpin (HH) to helix bundles (HBs) resembling a nematic droplet with the helices pointing along a director. We also show that the shape of the crowders has a profound influence on the structures that are populated. These entropically driven transitions depend on $N$, the number of beads in the polymer, size, and shapes of crowding particles as well as parameters describing the quality of the solvent. Our study illustrates how multiscale simulations can be performed for complex systems guided by concepts in polymer and colloid science.[24]

## METHODS

**Models.** We used a single homopolymer chain containing 16, 32, or 64 beads. The structural transitions are studied in the absence and presence of crowders, which are modeled either as spheres or rodlike polymers composed of spherical monomers. All beads in the polymer are identical and have the same van der Waals interactions with the other beads and the crowders. The potential energy of the polymer chain $E_p$ is given by the sum of the following terms

$$E_p = V_{bond} + V_{angle} + V_{dihe} + V_{vdW} \quad (1)$$

The potentials are chosen in the conventional form of the AMBER simulation package,[25] with the covalent bond and angle being harmonic potentials. The dihedral potential is a sum of harmonic terms. The energy function of the homopolymer chain is

$$V_{bond}(r) = \sum_{bonds} K_b(r - r_0)^2 \quad (2)$$

$$V_{angle}(\theta) = \sum_{angles} K_\theta(\theta - \theta_0)^2 \quad (3)$$

$$V_{dihe}(\phi) = \sum_{dihedrals} \gamma\varepsilon\left\{\left(1 + \cos\left(\phi + \frac{2\pi}{3}\right)\right) + (1 + \cos 3\phi)\right\} \quad (4)$$

$$V_{ij}^{(vdW)}(r) = \sum_{pairs} \varepsilon\left[\left(\frac{R_{ij}}{r}\right)^{12} - 2\delta\left(\frac{R_{ij}}{r}\right)^{6}\right], \quad R_{ij} = R_i + R_j \quad (5)$$

In the absence of $V_{dihe}(\phi)$, a standard model for polymers, the chain would undergo a collapse transition as $\delta$ increases. However, $V_{dihe}(\phi)$ favors the formation of expanded structures. Thus, in our model the low free energy structures are determined by a balance between these conflicting interactions even when $\phi_c$ is zero.

The energy scale of the potentials is given by the parameter $\varepsilon$ in the van der Waals potential (eq 4). We set $\varepsilon$ = 1 kcal/mol in all the simulations. The covalent bond and the bond angle potentials (eqs 2 and 3) are taken to be harmonic with the following constants: $K_b$ = 100 kcal/mol Å$^{-2}$ = 100$\varepsilon$ Å$^{-2}$, $r_0$ = 4 Å; $K_\theta$ = 20 kcal/mol rad$^{-2}$ = 20$\varepsilon$ Å$^{-2}$, $\theta_0$ = 105°. The dihedral potential (eq 4) is similar to that used in previous simulations of $\alpha$-helical proteins.[26,27] We introduced the dimensionless parameter $\gamma$, which is used to vary the strength of the dihedral potential with respect to $\varepsilon$, thus controlling the stiffness of the polymer backbone. If not, it is otherwise indicated $\gamma$ = 1.

The hydrophobicity of the monomers is modeled using van der Waals potential $V_{ij}^{(vdW)}(r)$ acting between pairs of particles of types $i$ and $j$. In our simulations, we have only two types of particles: monomers with $r_{mon}$ = 2 Å and crowders with $r_c$ (including rodlike crowders, which are constructed from spheres) which are varied for different simulations. The potential $V_{mon-mon}$ acts only between monomers that are separated by three or more covalent bonds. The parameter $\delta$ controls the strength of attraction between different monomers, which qualitatively mimics the quality of the solvent in the absence of crowding particles. Depending on the system, it is


dx.doi.org/10.1021/jp212535n | J. Phys. Chem. B 2012, 116, 8513−8522

varied in simulations from zero, which correspond to purely repulsive interactions, to unity.

*Crowders as Spherocylinders.* The rodlike (spherocylinder) crowder is constructed as a polymer with the same types of interactions as those for the helical polymer, except the dihedral interaction is absent and for all covalent angles $\theta = 180°$. Thus, all the monomers are roughly aligned in a line. Because the spherocylinders are not absolutely rigid, there are some fluctuations in covalent bond distance, and the bond angles fluctuate around the equilibrium values. The fluctuations in the bond angle lead to a slight curvature in the rods, which becomes more pronounced as the length of the spherocylinder increases. The radius for all rods is fixed at $r_{rod} = 4$ Å . For all the systems the covalent bond length of the rodlike particles is fixed at $b_{rod} = r_{rod} = 4$ Å, thus approximately modeling a spherocylinder. The shape asymmetry of the crowders is characterized by $L/D$, where $D$ is the diameter $= 2r_{rod}$ and $L$ is the distance between the centers of the first and the last monomers. Given our choice $b_{rod} = r_{rod}$, the number of monomers in a rod $N_{rod}$ is given by $N_{rod} = 2L/D + 1$.

**Simulation Details.** Simulations were performed with the AMBER simulations package[25] modified to run Langevin dynamics in the low-friction limit, which has been shown to enhance conformational sampling.[28] The velocity form of the Verlet algorithm is used, similar to that employed in previous publications.[4,26,27] The integration time step $\Delta t$ is chosen based on the oscillatory time of the covalent bonds $\tau$. The masses of all particles in the system (monomers and crowders) are set to one atomic mass unit. This yields the following covalent bond time $\tau = (m/K_b)^{1/2} = 0.0046$ ps. The integration time step is set to $\Delta t = 0.46$ fs $\approx 0.1\tau$.

For each system, ten runs are produced, each starting with a different initial conformation generated during the initial equilibration step. The simulation time for each run depends on the equilibration time (to obtain good statistics) and the number of particles in the system (to keep simulation times realistic). A typical number of time steps is $10^7$, with the variation between $10^7$ (high temperature, $N = 16$) and $9 \times 10^7$ (lowest temperatures, $N = 64$). From each run, 1000 snapshots are saved. The sampling rate is determined from the condition that different snapshots are statistically independent at the highest temperatures. The statistical inefficiencies $g$ (see, for example, ref 29) are used to measure statistical independence of snapshots. At high temperatures, the sampling rate is chosen so that $g \approx 1$. For higher temperatures, $g$ is kept <10 before the collapse of the chain into a globule. With the collapse of the chain, the equilibration times increase dramatically, so longer simulation times are used. The data presented at the lowest temperatures have $g < 100$, which corresponds approximately to 100 statistically independent snapshots from 10 runs. The usefulness of $g$ also decreases at low temperatures with the appearance of metastable states with relaxation times on the order of the simulation run time. To exclude this possibility, low-temperature runs are visually checked to make sure that the system explores a number of different configurations. We also start simulations from a number of metastable states identified for each particular case to ensure that their lifetimes are shorter than the simulation time.

For simulations with crowders, cubic periodic boundary conditions in the NVT ensemble are employed. For small radii of crowders, the simulation box size is equal to the length of the fully extended helix plus four average distances between crowders at a given volume fraction. The number of crowder $n_c$ for the smallest $r_c$ and $\phi_c = 0.2$ for $N = 16$ is ≈1200; for $N =$ *textbf*2, $r_c = 4$, $\phi_c = 0.2$: $n_c \approx 2000$; for $N = 64$, $r_c = 4$, $\phi_c = 0.2$: $n_c \approx 3000$.

The number of rods in the simulation box is calculated based on $\phi_c$ and using the volume of rodlike crowder $V_{rod}$ approximated as a spherocylinder $V_{rod} = 2\pi R^3((2/3) + (L/D))$. The simulation procedure is the same as for systems with spherical crowders. The box size is in all cases larger than the length of an expanded helix, varying between 165 Å (for $L/D = 1$) and 185 Å ($L/D = 4$) corresponding to the number of crowder monomers ≈4000 to ≈5600.

**Analysis.** To characterize the equilibrium states, we calculated the following properties.

*Radius of Gyration.* The dimensions of the polymer chain are characterized with the radius of gyration

$$R_g = \left\langle \left[ \frac{1}{2N^2} \sum_{i,j} (r_i - r_j)^2 \right]^{1/2} \right\rangle \tag{6}$$

*Helical Content.* We define average helicity as a fraction of dihedral angles in a "helical state". Each dihedral angle is defined to be in a helical state if the value of the angle $|\phi_i - \phi_i^N| < \Delta_H$, where $\Delta_H = 12.07°$; otherwise, the dihedral angle is counted as being in a "nonhelical state". With these definitions, the overall degree of helicity is

$$H = \frac{1}{N-3} \sum_{i=1}^{N-3} \langle \Theta(\Delta_H - |\phi_i - \phi_i^N|) \rangle = \frac{1}{N-3} \sum_{i=1}^{N-3} h_i \tag{7}$$

where $\Theta(x)$ is a Heavyside function. The choice of $\Delta_H = 12.07°$ will be discussed below.

We also considered a two-dihedral angle measure for helicity, $H_2$, which is defined as the fraction of two consecutive dihedral angles, both of which are in a helical state as defined by the native conformation

$$H_2 = \frac{1}{N-4} \sum_{i=1}^{N-4} \Theta(\Delta_{H2}\phi - |\phi_i - \phi_i^N|) \Theta(\Delta_{H2}\phi - |\phi_{i+1} - \phi_{i+1}^N|) \tag{8}$$

Note that in this definition we use a different numerical value of deviation in the dihedral angle $\Delta_{H2}$. We choose $\Delta_{H2} = 20.31°$ for reasons to be discussed below. The use of $H_2$, which compares the fate of two consecutive dihedral angles, ensures that at least 1.5 helical turns are formed. All averages are calculated using an ensemble of trajectories.

## RESULTS

**Diagram of States in the $\gamma$–$\delta$ Plane.** We first characterize the nature of structures in the absence of crowding particles. The internal stiffness of the chain, favoring chain expansion, can be altered by changing $\gamma$ (eq 4), while the extent of collapse can be controlled by altering $\delta$ (eq 5), the surrogate parameter for controlling the quality of solvent. The existence of different states is ascertained using the order parameter $R_g/R_g^H$. We classify the regions of $\delta$–$\gamma$ parameter space according to the behavior of $R_g/R_g^H$ observed in simulations of the polymer chain with $N = 16$. At low $\delta$ and high $\gamma$, $R_g$ increases monotonically with decreasing $T$, a signature of the coil–helix transition. In the intermediate $\delta$ range, $R_g$ passes through a maximum before decreasing as $T$ is lowered. In this case, the helical content of


dx.doi.org/10.1021/jp212535n | J. Phys. Chem. B 2012, 116, 8513–8522

the coil increases significantly before condensing into helical hairpin (HH) structures. As $\delta$ is increased further, the solid $R_g$ decreases monotonically as $T$ is lowered. The states in this regime can be thought of as a coil−globule transition with a high degree of helicity in the globule.

For a fixed $\gamma$ (unless stated otherwise, $\gamma$ is fixed to unity from now on), we can roughly associate solvent quality in terms of $\delta$ (eq 5). Although such a classification has to be done precisely for each $N$, we surmise that $\delta \leq 0.2$ corresponds to a good solvent, whereas when $\delta$ exceeds 0.5 the solvent is poor so that the polymer would be collapsed even in the absence of crowders. In the range $0.2 < \delta \leq 0.5$, the solvent is moderately poor and could be in the cross over Θ-like regime. The influence of the crowding particles on the structural transitions depends on a number of factors including $N$, the size, shape, and volume fraction of crowding particles as well as $\delta$.

**Structural Transitions in Polymers in the Absence of Crowders As a Function of *N* and δ.** We plot in Figure 1 the

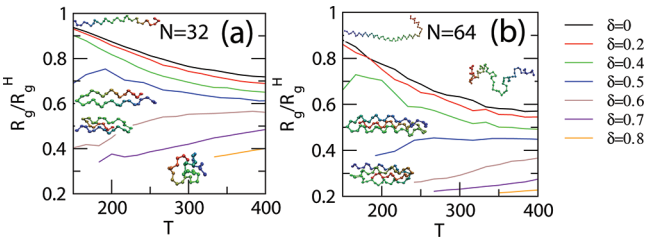


**Figure 1.** Normalized radius of gyration as a function of $T$ for $N = 32$ (a) and $N = 64$ (b) polymer chains. Different curves are for different values of the attraction parameter $\delta$. The values of $\delta$ are given on the right.

normalized radius of gyration $R_g/R_g^H$ ($R_g^H$ is the radius of gyration of the energy minimized helix) for $N = 32$ and $N = 64$. Different curves in the plots refer to simulations with different values of the monomer−momomer attraction parameter $\delta$ (defined in eq 5). The value of $\delta$ changes from 0 (purely repulsive interaction between monomers) to $\delta = 1$ (corresponding to poor solvents). From the plots of $R_g$ in Figure 1, we can identify three different behaviors of $R_g$ as $T$ is changed, depending on the magnitude of $\delta$. At low $\delta$, the high $T$ disordered random coil conformations undergo a transition to a well-ordered helix when $T$ decreases. In this case the intrinsic stiffness due to the dihedral angle potential dominates over attractions between monomers. Consequently, there is a monotonic increase in $R_g$ with decreasing $T$ (Figure 1).

At intermediate values of attraction (e.g., $\delta \approx 0.5$ for the $N = 32$), the high $T$ random coil first expands into a conformation with significant helical content (thus having larger $R_g$) before collapsing into a hairpin for $N = 16$[22] and HBs for larger $N$. The sequence of structural transitions that occurs as $T$ and $\delta$ are altered is shown in Figure 1 using conformations that represent random coil, collapsed globule, HHs, and HBs. The observed structural transitions are manifested by an increase in $R_g$ at lower $T$ and then a sharp decrease in $R_g$ corresponding to the collapse into hairpin-like structures, depending on $\delta$ (see, for example, the curves for $N = 32$, $\delta = 0.5$, and $N = 64$, $\delta = 0.4$ in Figure 1).

As the solvent quality becomes poor ($\delta$ exceeds 0.6), the values of $R_g$ decrease monotonically with decreasing $T$, which is observed, for example, for $\delta = 0.7$ in Figure 1. In this case, the structures are compact with significant helical content. We show below that even the collapsed globule still has a rather high degree of helicity. These results show that the diagram of states for an isolated polymer is rich and is determined by $T$, $N$, and $\delta$ for a fixed $\gamma$.

**Transitions between Coil, HH, and HB Controlled by *δ*.** The probability distribution functions of $R_g/R_g^H$ for three values of $\delta$ at different temperatures for $N = 32$ corresponding to the three regimes describing the solvent quality are shown in Figure 2. For $\delta = 0$ at high $T$, the distribution is broad with expanded coil conformations (although still with a rather high helical content). With decreasing temperature, the distribution narrows, and the maximum shifts to near unity, indicating the formation of a fully extended well-defined helix. We do not find any evidence for coexistence between a coil and a helix as $T$ is changed.

For intermediate $\delta = 0.5$ at high temperatures, we observe a broad random coil distribution, similar to the $\delta = 0$ case. However, when the temperature is decreased, there is a broadening of the distribution and then emergence of separate peaks corresponding to coexisting expanded helix, HH, and three-helix bundle (HB) structures.

A different picture emerges in the poor solvent case ($\delta = 0.7$), which corresponds to the regime of monotonically decreasing $R_g$ with decreasing $T$. In this case, even at high $T$ the conformations are already collapsed. They are further compacted with decreasing temperature, with the most

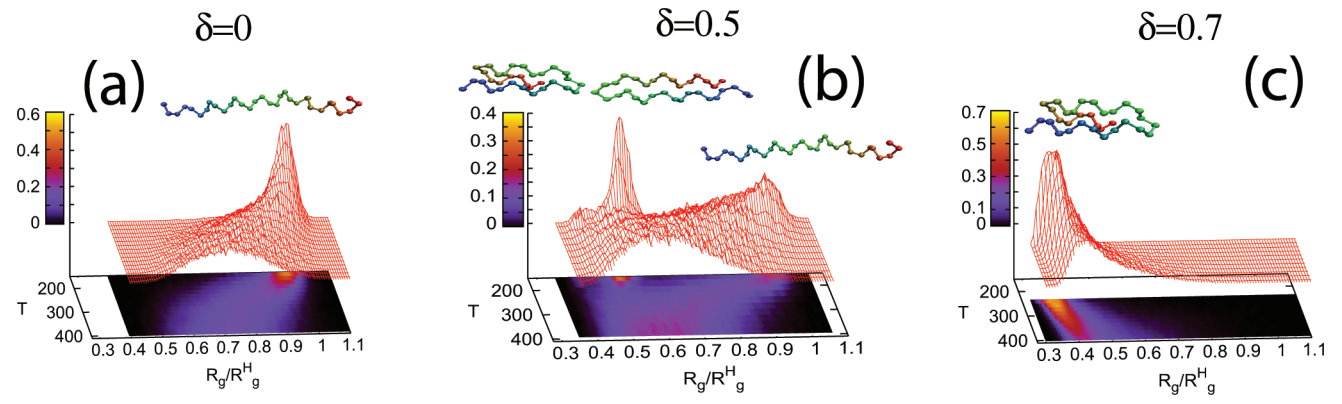


**Figure 2.** Temperature-dependent changes in the probability distribution of $R_g/R_g^H$ for $N = 32$. (a) $\delta = 0$; (b) $\delta = 0.5$; (c) $\delta = 0.7$. Typical conformations corresponding to the peaks in the $R_g/R_g^H$ probability are shown. Note a different scale in the $z$-axis, in the three plots.


dx.doi.org/10.1021/jp212535n | J. Phys. Chem. B 2012, 116, 8513−8522

dominant conformation being a HB. As in the case of $\delta = 0$, no coexistence between different conformations is observed.

**Dependence of Transition Temperatures As a Function of $\delta$.** A number of different definitions can be used to estimate the structural transition temperature $T_S$. Because we are mostly interested in the helical content during the structural transitions, we used $H(T_S) = 0.5$ (eq 7) or $H_2(T_S) = 0.5$ as the definition of $T_S$. The values of tolerance for deviations from an ideal helix for $H$ and $H_2$ are chosen so that the calculated $T_S$ values match that obtained from the maximum of $C_V$ for the longest polymer chain of $N = 64$ at $\delta = 0$. The transition temperatures using $H$ and $H_2$, once parameters $\Delta_H$ and $\Delta_{H2}$ are chosen appropriately, lead to almost identical $T_S$. In what follows, we report $T_S$ determined from the condition $H(T_S) = 0.5$.

We calculated[22] the dependence of $T_S$ on the strength of monomer attraction $\delta$ for 16, 32, and 64 bead polymers. For all $N$, the transition temperature decreases with increasing attraction with the decrease being more pronounced for longer chains. As discussed in relation to Figure 1, the decrease in $T_S$ is a manifestation of the growing compaction of polymers at higher $\delta$, which maximizes the number of monomer contacts. In the process, the degree of helical order is altered. With increasing $\delta$ helicity $H$ monotonically decreases for all $T$. The decrease in $T_S$ can be understood by noting that the stability of the compact structure increases as $\delta$ increases. If we assume that the free energy of the ordered structures does not change significantly as $\delta$ increases, then the decrease in the transition temperature is approximately given by $k_B\Delta T_S \approx -\Delta G_c(\delta)$ where $\Delta G_c(\delta)$ is the additional stabilization of the coil state due to increasing strength of the monomer−monomer attraction. The decrease in $T_S$ in the absence of crowding particles depends on a number of factors including the value of $\delta$.

**Monodisperse Spherical Crowders.** We report the results of simulations of the shorter and longer polymer chains ($N = 16$ and 64) in the presence of crowding particles modeled as spheres that have purely repulsive interactions between themselves and also with the monomers. We are primarily interested in the effect of crowding on the helical structural transitions as $\delta$ is varied. For $\delta = 0$, which corresponds to good solvent conditions, the polymer is a random coil at high temperatures. The transition to a helical state occurs at low temperatures (Figure 3). For this case, we expect that the crowding particles will decrease the entropy of the coil state, thus entropically stabilizing the helical states, HH, and HB states as predicted in a number of studies. Thus, for $\delta = 0$ we expect $T_S$ to increase in the presence of crowding particles[4] as found experimentally.[30] For $\delta \neq 0$ the lowest free energy structures are determined by a balance between a number of factors, as discussed above.

Because much less is known about crowding-induced structural transitions in poor solvents or in nearly poor solvents, we choose for each polymer chain the interaction parameter value ($\delta$) such that the uncrowded polymer forms a helix at low temperatures. In each case, $\delta$ was chosen, based on the results in the absence of crowding particles, such that it is close to the crossover value, beyond which the low-temperature conformations are collapsed into a hairpin. Accordingly, we choose $\delta = 0.5$ for $N = 16$ and $\delta = 0.3$ for $N = 64$.

The dependence of $R_g/R_g^H$ on $T$ for systems in the presence of spherical crowding particles is displayed in Figure 3. Plots (a) and (b) are for $N = 16$, and plots (c) and (d) are for $N = 64$. For each chain we performed two sets of simulations. In

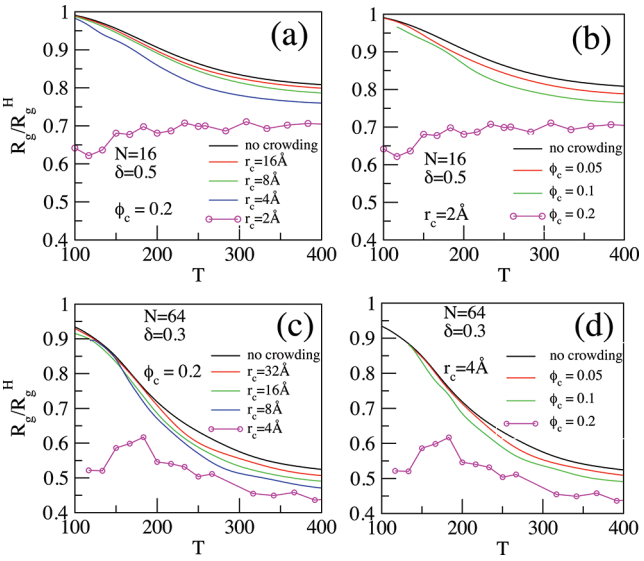


**Figure 3.** Normalized radius of gyration $R_g/R_g^H$ as a function of $T$ in the presence of crowders. $R_g^H$ is the value of the radius of gyration of the energy minimized structures. (a) Effect of crowder radius $r_c$ (values given in the plot) at a constant crowder volume fraction $\phi_c = 0.2$ on structural transitions in the $N = 16$ chain with $\delta = 0.5$. (b) Varying $\phi_c$ at a constant $r_c = 2$ Å for $N = 16$, $\delta = 0.5$. Plots (c) and (d) explore effects of varying $r_c$ and $\phi_c$, respectively, for a longer chain, $N = 64$, with $\delta = 0.3$.

Figures 3(a) and 3(c), the volume fraction of crowders is kept constant at $\phi_c = 0.2$, and the radius of crowders $r_c$ is varied. The results obtained by varying volume fractions $\phi_c$ for a $r_c = 2$ Å for the $N = 16$ chain and $r_c = 4$ Å for $N = 64$ are in Figures 3(b) and 3(d), respectively.

It is instructive to compare the effect of crowding in Figure 3 to the effect of increasing $\delta$ for isolated chains (Figure 2 and ref 22). Comparison of the results in these figures shows that qualitatively the addition of crowders is equivalent to increasing the effective monomer−monomer attraction. This conclusion is valid for all regimes discussed previously: weak attraction, when the low-temperature configuration is an expanded helix; and higher $\delta$ when the polymer chain collapses at low $T$ into hairpin and HB structures. We observe that given the sufficiently high value of the bare attraction $\delta$ crowding can induce collapse into hairpins at low temperatures. Physically crowding induces intramolecular depletion attraction that arises because the crowding particles are excluded from the overlap zone surrounding two monomers. The entropic nature of the depletion attraction, known as Asakura−Oosawa (AO) force,[31] results in the renormalization of the bare $\delta$ to $\delta_{eff} = \delta + f(\phi_c, r_c)$[32] where $f(\phi_c, r_c)$ is an increasing function of the volume fraction, $\phi_c$, of the crowding particles. Thus, even with $\delta = 0$, crowding can cause collapse the polymer,[33−36] which in our case leads to formation of various ordered structures. The arguments given here are only qualitative because crowding agents multiparticle interactions,[32] which cannot be captured using only $\delta_{eff}$.

We can infer from Figures 3(a) and 3(c) that, at a given $\phi_c$ and $T$, the effective crowder-induced monomer−monomer attraction increases as the size of the crowding particles decreases. In addition, Figures 3(b) and 3(d) show that for a fixed size of the crowding particle, $r_c$, the effective monomer−monomer attraction increases with the increase of $\phi_c$. These


dx.doi.org/10.1021/jp212535n | J. Phys. Chem. B 2012, 116, 8513−8522

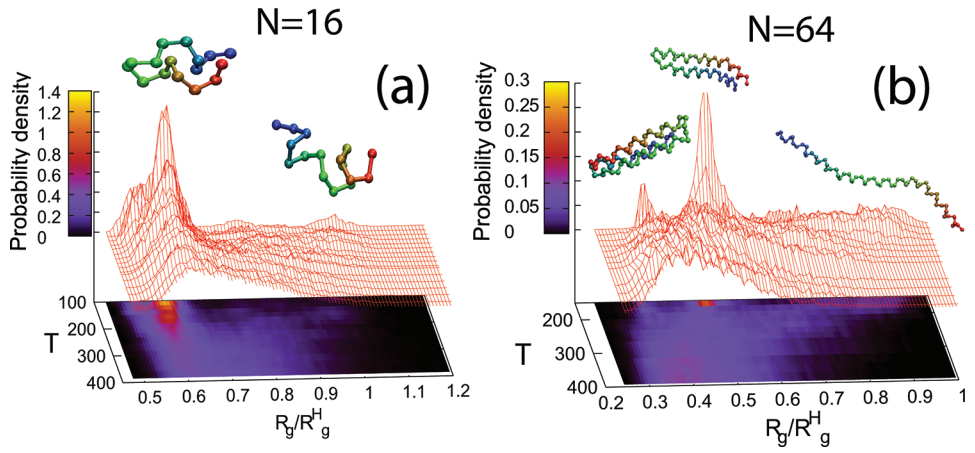


**Figure 4.** Changes in $R_g/R_g^H$ probability density as a function of $T$ for the two systems of Figure 3 with the greatest effect of crowding. (a) $N = 16$, $\delta = 0.5$; $r_c = 2$Å, $\phi_c = 0.2$. (b) $N = 32$, $\delta = 0.3$; $r_c = 4$Å, $\phi_c = 0.2$. The structures of crowding-induced HH and HB are also shown.

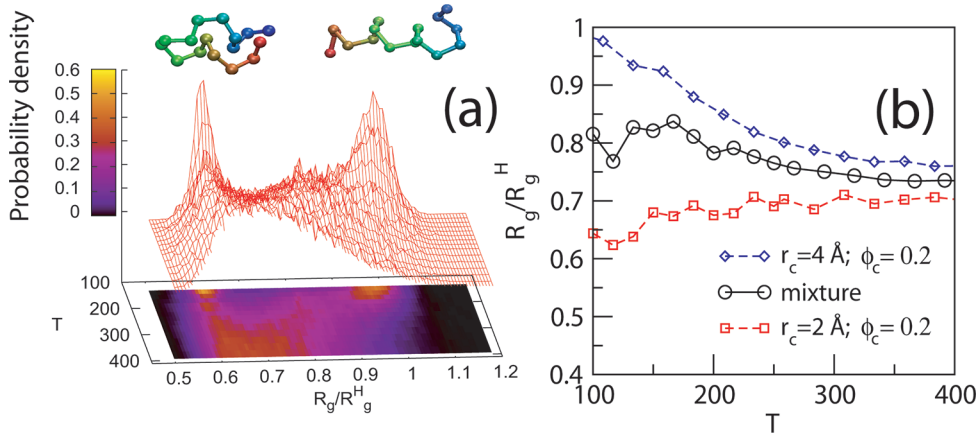


**Figure 5.** Mixture of two crowders $r_{c1} = 2$ Å, $r_{c2} = 4$ Å and $\phi_{c1} = \phi_{c2} = 0.1$ for an $N = 16$ chain with $\delta = 0.5$. (a) Temperature-dependent changes in the distribution of $R_g/R_g^H$. (b) Average $R_g/R_g^H$ as a function of $T$ for the mixture (circles as indicated in the plot). The corresponding results for the one-component systems at $\phi_c = 0.2$ are shown for reference.

conclusions are qualitatively valid for all $N$, although the strength of the effective interaction depends on $r_c$.

From the AO theory,[31] which like other treatments is also only approximate, it can be shown that the strength of the depletion attraction, whose range is $r_c$ (for hard crowding particles), is proportional to $\approx(1/r_c^3)$. Thus, small crowding particles are more effective in compacting the polymer[8] even though the range of attraction is diminished. The AO theory only qualitatively explains the simulation results. At low volume fractions $\phi_c$ and large $r_c$ (coil−helix transition regime), the effect of crowding is mostly to make expanded random-coil structures at high $T$ more compact (Figure 3), which is roughly equivalent to increasing the bare $\delta$. The presence of crowders has a smaller effect on the fluctuating helix at lower $T$.

In Figure 4, we plot the distribution functions $P(R_g/R_g^H)$ for the two cases in Figure 3 with the highest effect of crowding: $N = 16$ with $r_c = 2$Å, $\phi_c = 0.2$ (Figure 4(a)), and $N = 64$ with $r_c = 4$Å, $\phi_c = 0.2$ (Figure 4(b)). In the absence of crowders, in both cases where the helix−coil type of transition takes place, the $P(R_g/R_g^H)$ values are similar to that in Figure 2(a) for $N = 32$. Crowding particles induce additional effective attraction leading to the emergence of hairpin-like structures. For $N = 16$, the dominant structure is a hairpin (Figure 4(a)) that coexists with an extended helix. In the $N = 64$ case, shown in Figure 4(b), the dominant structure at low $T$ is a HH, which coexists with a HB and an extended helix.

**Mixtures of Spherical Crowders.** We consider a model system of crowders that contain a binary mixture of spherical particles. In the binary mixture the composition of the individual component is as an additional variable that can affect the structural changes in the polymer. We study the helical transitions in a number of binary mixtures of spheres and look at the effects of variation of the crowder radius and the volume fraction of the components in the mixture. The simulation procedure is the same as in the previous case. We choose the size of the simulation box using the condition that it should accommodate a fully extended helix plus several average intercrowder distances. To satisfy these criteria, we used simulation boxes containing 1200−1800 particles for the systems studied. To ensure that conformations of the polymer and the associated configurations of the crowding particles are adequately sampled, we restricted these simulations to $N = 16$.

The attraction parameter for all simulations is $\delta = 0.3$. As discussed previously,[22] without crowders the polymer with $\delta = 0.3$ adopts an extended helix conformation with decreasing temperatures. In the presence of monodisperse spherical crowding agents, the largest effect of crowding is observed for $r_c = 2$Å, $\phi_c = 0.2$ (Figure 3(a)), for which the low-temperature conformation is dominated by the HH (Figure


dx.doi.org/10.1021/jp212535n | J. Phys. Chem. B 2012, 116, 8513−8522

4(a)). For a larger radius of $r_c$ = 4 Å at the same volume fraction, the dominant low $T$ conformation is an extended helix.

We simulated the conformational changes of the $N$ = 16 polymer in a 50:50 mixture (by volume) containing crowding particles with $r_{c1}$ = 2 Å, $r_{c2}$ = 4 Å, and $\phi_{c1} = \phi_{c2}$ = 0.1. (In this system, we do not observe phase separation of crowders at any temperature.) Figure 3 and arguments based on AO theory show that increasing the crowder radius diminishes their effects on the coil−helix transition. This is indeed what we observe in Figure 5(a), which shows that at low temperatures the probabilities of finding the polymer in a HH or extended helix conformation are comparable. This can be qualitatively rationalized as a result of superposition of probability distributions of the two reference one-component systems: $r_c$ = 2Å, $\phi_c$ = 0.2 and $r_c$ = 4Å, $\phi_c$ = 0.2. The averaged $R_g/R_g^H$ plotted in Figure 5(b) for the mixture (solid black lines) and the two reference systems (dashed lines in Figure 5(b)) demonstrate that, at least for this particular system, even quantitatively the conclusion holds true. One can obtain the $R_g/R_g^H$ results for the mixtures, simply by averaging the values for the components comprising the mixture, a result that has general applicability.[10,37]

We also tested the effects of varying the composition of the second components on the coil−helix transition. The probability distributions of $R_g/R_g^H$ at low and high $T$ obtained by changing $r_{c2}$ and $\phi_{c2}$ are shown in Figure 6. In these

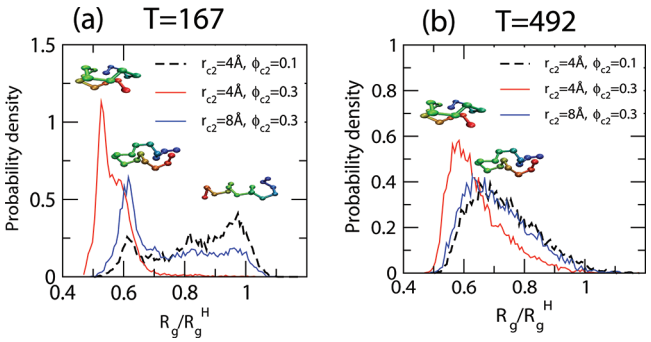


**Figure 6.** Probability distributions of $R_g/R_g^H$ for three different mixtures of crowders at low and high temperatures. For all systems, $r_{c1}$ = 2 Å and $\phi_{c1}$ = 0.1. The second component, as indicated in the plots, is $r_{c2}$ = 4 Å, $\phi_{c2}$ = 0.1 (dashed black line); $r_{c2}$ = 4 Å, $\phi_{c2}$ = 0.3 (red line); $r_{c2}$ = 8 Å, $\phi_{c2}$ = 0.3 (blue). Plots (a) and (b) are for $T$ = 167 and $T$ = 492 K, respectively.

simulations, we keep the first component constant at $r_{c1}$ = 2Å, $\phi_{c1}$ = 0.1 and vary the properties of the second component. Let us start with a mixture with $r_{c1}$ = 2 Å, $r_{c2}$ = 4 Å, and $\phi_{c1}$ and $\phi_{c2}$ = 0.1 (dashed black line in Figure 6) and increase the volume fraction of the second component to $\phi_{c2}$ = 0.3. Figure 6 shows that the polymer is compact at both low and high temperatures. At the low temperature, the dominant conformation can be thought of as compact, but deformed HH containing defects arise from an increase in the number of intrapolymer contacts. The more ideal HH is also discernible in the probability distribution (Figure 6) as a shoulder, especially at the low temperature (the peak at $R_g/R_g^H \approx 0.57$ in Figure 6). The extent of polymer compaction due to crowding is larger at the higher volume fraction of 0.4 than for the one-component system $r_c$ = 2Å, $\phi_c$ = 0.2. At the high temperature, the probability distribution also has a maximum at a value of $R_g/R_g^H$ corresponding to the population of the deformed HH. The distribution is shifted to more compact conformations compared with the black dashed curve calculated using $r_{c2}$ = 4 Å, $\phi_{c2}$ = 0.1 (see Figure 6(b)). These conclusions are consistent with the expected result that increasing the crowder volume fraction leads to a greater polymer compaction.

We increased the radius of the second component to $r_{c2}$ = 8 Å, keeping $\phi_{c2}$ = 0.3. As expected, the increase of $r_c$ leads to diminished crowding effects found in the one-component systems. At $T$ = 167 K the dominant conformation is the HH (blue curve in Figure 6a), with the distribution that resembles the one for $r_c$ = 2 Å, $\phi_c$ = 0.2 (Figure 4a). For the higher $T$ (Figure 6(b)), the distribution shifts to less compact conformations as well. On the basis of these results, we conclude that the trend regarding the variation of $r_c$ is valid for mixtures in the same manner as for one-component systems. In other words, the smaller crowding particles (more precisely $(r_c/R_g^H) \leq 1$) have a greater influence because they induce stronger intramolecular AO depletion attraction.

We note parenthetically that in the system ($r_{c1}$ = 2 Å and $r_{c1}$ = 8 Å) at $T$ = 167 K the crowders phase separate. The polymer is localized predominantly in the phase containing the smaller ($r_c$ = 2 Å) crowding particles. However, the phase separation does not lead to any new features in the crowder-induced polymer compaction. The probability distribution in Figure 6(b) is consistent with diminished crowding effects for a larger $r_{c2}$.

**Crowders as Spherocylinders.** To elucidate the effect of the shape of crowders on the polymer conformations at low and high temperatures, we performed simulations containing monodisperse rodlike (more precisely spherocylinders) crowding particles and varying aspect ratio $L/D$. We chose $N$ = 64 with $\delta$ = 0.3 and the volume fraction of the spherocylinders, $\phi_c$ = 0.2. Systems with $L/D$ = 1, 2 and 4 $L/D$ = 1, 2, and 4 are studied. For each $L/D$, we performed simulations at $T$ = 167 K and $T$ = 492 K to study the effects of rodlike crowders on mostly helical and mostly disordered conformations, respectively. Instead of fixing $\phi_c$ and varying the volume per particle, one could simulate a system with both $\phi_c$ and the volume per particle (regardless of their shape). This will result in variations in the number density. Because on theoretical grounds it is $\phi_c$ that is crucial for hard crowding particles, we studied the shape effects by fixing $\phi_c$.

The probability density distributions of $R_g/R_g^H$ and the averaged values of $R_g/R_g^H$ and helix content for the polymer in the presence of spherocylinders are shown in Figure 7. Let us consider the results for $T$ = 167 K, presented in Figures 7(a) and 7(b). In the absence of crowders, the most probable polymer conformation is a well-formed helix, with the maximum in $R_g/R_g^H$ distribution slightly less than unity, as is clear from the $R_g/R_g^H$ distribution (dashed violet line in Figure 7(a)). Addition of spherical crowders ($L/D$ = 0, thick black line) leads to collapse of the extended helix into a HH and a three HB being the most probable conformations (cf. Figure 4(b)).

In contrast to spherical crowders ($L/D$ = 0), spherocylinders have a drastically different effect on the structures of the polymer. Even for $L/D$ = 1 we see that the extended helical conformation is dominant in contrast to HH and HB that are populated in the presence of spherical crowders. The peaks for HH ($R_g/R_g^H \approx 0.3$) and three helix bundle ($R_g/R_g^H \approx 0.5$) conformations, while still distinctly present (Figure 7a), are strongly suppressed. For crowders with $L/D$ = 2 and 4 the results are almost identical, which allows us to extrapolate them


dx.doi.org/10.1021/jp212535n | J. Phys. Chem. B 2012, 116, 8513−8522

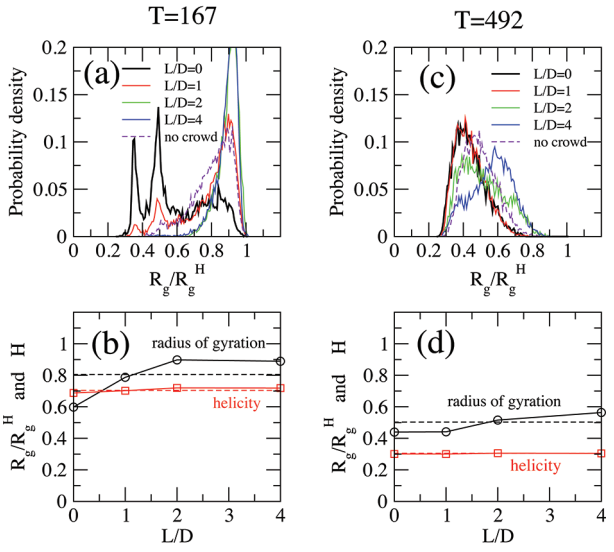


**Figure 7.** Effect of the aspect ratio $L/D$ spherocylinders on the structures of $N = 64$ polymer, at constant crowder volume fraction $\phi_c = 0.2$ and diameter $D = 4$ Å. (a) and (c) give the probability distributions of $R_g/R_g^H$ for different values of $L/D$ parameter for $T = 167$ K and $T = 492$ K, respectively. Results for spherical crowders ($L/D = 0$) are in a thick black line, and a system without crowders (dashed violet line) is also shown for reference. (b) and (d) $R_g/R_g^H$ (black circles) and helix content $H$ (red squares) as a function of $L/D$ for the same two temperatures $T = 167$ K and $T = 492$ K. Dashed black and red lines are reference values of $R_g/R_g^H$ and $H$, respectively, in a system without crowders.

into the nematic region of higher $L/D$ values. In these cases the extended conformation is even more dominant than is the case in the absence of crowders. As the aspect ratio increases, the polymer fluctuations are greatly suppressed by the rodlike crowding particles resulting in the formation of the helical conformation as the most lowest free energy state (see below for a physical explanation).

The average values of $R_g/R_g^H$ and $H$, presented in Figure 7(b), reflect the spherocylinder-induced conformational changes in the polymer. The average $R_g/R_g^H$ at $L/D = 0$ is smaller than that obtained at $\phi_c = 0$ and increases monotonically with increasing $L/D$ (black circles in Figure 7b). Already at $L/D \approx 1$, the radius of gyration is equal to that of the no-crowder system (although the underlying conformations are slightly different). With further increase in $L/D$, the average $R_g/R_g^H$ increases and appears to saturate for $L/D \geq 2$. The variation in the helix content $H$ is much smaller (compare dashed and red lines in Figure 7b), which is in agreement with the conformational changes observed in Figure 7(a).

Thus, the effect of rodlike crowders ($L/D > 1$ for our case) at low temperatures is to destabilize the collapsed HH-like conformations. At higher aspect ratios, bending fluctuations of a well-formed helix, which are present at $\phi_c = 0$ and in the presence of spherical crowders, are suppressed leading to the formation of a nearly ideal helix with a sharp peak in the distribution of $R_g/R_g^H$ at $R_g/R_g^H \approx 0.9$. The average value of $R_g/R_g^H$ is fairly close to that for an ideal helix. A similar but much less dramatic trend holds at $T = 492$ as well (Figures 7(c) and (d)). The probability density shows that, without crowders, the system is a disordered "random" coil (peak in $R_g/R_g^H \approx 0.5$). Addition of spherical crowders results in chain compaction as shown by a shift in $R_g/R_g^H$ to ≈0.4. A change of the crowder shape to a rod with $L/D = 1$ does not have a perceptible effect on the system, with the $R_g/R_g^H$ lying virtually on top of the spherical crowders one. A further increase to $L/D = 2$ and 4 leads to a shift in the distribution of $R_g/R_g^H$ to more extended conformations with larger $R_g/R_g^H$. Correspondingly, the average of $R_g/R_g^H$ in Figure 7(d) increases with increasing $L/D$. In this case the average $R_g/R_g^H$ does not saturate at larger $L/D$. We expect further chain expansion as the spherocylinders make transition to a nematic phase at higher $L/D$ and $\phi_c$. The changes in the helicity, which is low at high $T$, are negligible.

**Nematic Phase of the Rodlike Crowders and Polymer Helix Formation.** The overall picture that emerges is that the spherocylinders lead to an expansion of the polymer leading to a nearly ideal helical state especially at low temperatures. Because these crowding particles can undergo a transition to a nematic phase at high enough $\phi_c$,[38] it is of interest to ascertain if such a transition leads to the predominant formation of an ideal hairpin over HH and HB found in the presence of spherical crowders (Figure 6). To understand the connection to a possible nematic liquid crystal formation in the crowding particles, we analyzed the eigenvalues of the orientation tensor

$$\langle Q_{\alpha\beta}(R)\rangle = \left\langle \frac{1}{n(R)} \sum_{i,j=1}^{n(R)} u_\alpha^{(i)} u_\beta^{(j)} \right\rangle \quad (9)$$

defined for number $n(R)$ rods, which are closer than a certain distance $R$ to the polymer. In eq 9, $u_\alpha^{(i)}$ is the $\alpha$ component of the unit vector along the $i$th rod. For each distance $R$ we calculate the tensor for $n(R)$ rods only if the center of the rod is $\leq R$ from any polymer monomer. The largest eigenvalue $I_3(R)$ of $Q_{\alpha\beta}$ is used to define the nematic order parameter $P_2(R) = (3I_3(R) - 1)/2$.

The systems studied here do not exhibit nematic ordering ($P_2(\infty) < 0.1$ for all $L/D$ simulated). In other words, the volume fraction is far less than that needed for formation of a nematic phase. However, we find that $P_2(R)$ increases in the vicinity of the polymer (small $R$) at high and low temperatures, with the effect being more pronounced for higher $L/D$. Analysis of the correlations between the eigenvector associated with $I_3$ and the eigenvector along the long axis of the gyration tensor of the polymer shows preferential orientation of the rods in the direction of the long polymer axis. Thus, the elongation of the polymer conformations observed at $T = 167$ and 492 K is due to local partial nematic ordering of the spherocylinders in the vicinity of the polymer. The ordering is induced by the presence of the polymer chain, which introduces the preferred direction along the polymer in the expanded conformations. These expanded conformations are stabilized by the local partial nematic ordering of the spherocylinders. The coupling between the local ordering of the crowding particles and the polymer chains renders the helical state stable as the aspect ratio increases. It should be noted that transitions to HH and HB could occur at high $L/D$ ratio if $\delta$ is increased.

## ■ CONCLUSIONS

The diagram of states of a polymer in the presence of crowding particles is determined by a number of factors such as the solvent quality parametrized by $\delta$, shape, size, volume fraction, and polydispersity of the crowders. Only when $\delta$ is small, the ESM predicting enhanced stability of the ordered states with an increase in the ordering temperature, $T_S$, with increasing $\phi_c$ is expected.[4] For $\delta \neq 0$, describing a range of solvent quality


dx.doi.org/10.1021/jp212535n | J. Phys. Chem. B 2012, 116, 8513−8522

(moderately poor (Θ-like) or poor), crowding-induced structural transitions and the changes in the dependence of $T_S$ on $\delta$ can be complicated.[22] Here, we have shown that for a homopolymer, in the absence of crowders, an increase in $\delta$ leads to the formation of HH (for $N$ = 16) and multiple HBs (for $N$ = 16, 32, 64). The character of the transitions changes with increasing $\delta$ from coil−helix to globule−helix. In a sufficiently poor solvent (large $\delta$), the helix content of the low $T$ globule-like conformations can be less than what is found at moderate values of $\delta$. This occurs because the energy of the polymer can be minimized by increasing the number of contacts between monomers which can only be achieved at the cost of reducing the helical content favored by the stiffness associated with the dihedral angle potential. As a corollary, we predict that if $\gamma$ (Figure 1) is increased the helical structures would remain stable over a wider temperature range even if $\delta$ is increased.

In the presence of spherical crowders, there is an increase in the extent of collapse of the polymer at all temperatures, which is due to an increase in $\delta$ arising from the depletion effect. The changes in polymer conformations are similar to those observed in the system without crowders but occur at higher effective $\delta$. Thus, introduction of spherical crowders favors more compact conformations and destabilizes the helical structure. As a result, in contrast to the small $\delta$ regime, the structural transition temperature $T_S$ (defined using the average helicity of the polymer) is lower for a system with crowders than for the isolated polymer ($\phi_c$ = 0). The transition temperature $T_S$ decreases (signifying a greater helix destabilization due to crowding effects) with decreasing radius of spherical crowder $r_c$ and increasing volume fraction $\phi_c$. Introduction of spherical crowders can also induce formation of the HH and HB helix at low temperature in a polymer, which in the absence of crowders forms only an extended helix at low temperatures.

In the mixtures of two spherical crowders, the qualitative conclusions remain the same. Crowding induces effective monomer attraction which prefers compact structures with a higher number of monomer contacts and destabilizes helical structures especially when $\delta$ is large. The structural transition temperature decreases with increasing $\phi_c$ and decreasing $r_c$ of one crowding component, keeping the properties of other components constant at moderate and high $\delta$ values.

The results for mixtures also point to an interesting conclusion regarding explicit solvent. If we consider that the small $r_c$ component represents explicit solvent and the particles with larger $r_c$ are spherical crowding particles, then our results show that replacing half (by volume) the crowders with spheres of a larger size leads to a decrease in the effective attraction $\delta$. This result indicates a possibility of a complex scenario for crowding-induced structural transition, when the effective large crowder attraction on the polymer is counterbalanced by the modification in the solvent-mediated monomer interaction. A similar scenario has been explored in the context of collapse of coil in a mixture of athermal solvents.[39]

We also studied the effect of changing shape of crowders, by keeping the crowder volume fraction $\phi_c$ constant and building rodlike crowders out of spherical crowders. Surprisingly, at all temperatures the increase in $L/D$ leads to chain expansion, which is evident even at $L/D$ as low as 2. At low temperatures the expansion is favored due to destabilization of the collapsed hairpin conformations. At higher temperatures when conformations are mostly disordered, the elongation is due to stabilization of extended conformation, which exhibits a preferred direction along the polymer. In both cases we observe local, polymer-induced nematic order with the nematic director orienting preferentially along the long axis of the polymer. Remarkably, for $N$ = 64, HH and HB structures are completely destabilized. It would be of interest to further explore the $N$-dependence of the phase diagram in the presence of spherocylinders.

In this study, we have assumed that the crowding agents are monodisperse. The effect of polydispersity for spherical crowding agents has been treated earlier.[10] It would be interesting to consider polydispersity effects of rodlike particles on the stability of ordered structures. As pointed out elsewhere,[4,8] crowding has a maximum effect if the size of the crowding agents is less than that of the protein. In the opposite limit the stability becomes independent of the size of the crowding particle. Thus, if the crowding is a mixture of rods of differing sizes then the smallest spherocylinder would have the maximum effect on the stability. In addition, by appealing to previous studies[10,37] we suggest that the effect on stability would be additive and be determined by the partial volume fraction of the different components (classified by size) of the rod particles. Explicit simulations are needed to test this conjecture.

The use of coarse-grained models to describe complex problems involving multiple length and energy scales is becoming increasingly common. The present article presents a case study of the structural transitions that a polymer undergoes as the size, shapes, and volume fraction of the crowding particles are changed. There is a remarkable complexity in the structures that the polymer adopts depending upon the nature of crowding agents, solvent quality, and temperature. A plausible lesson from this study for the effects of crowding on the self-assembly of proteins and RNA is that there are multiple scenarios. For example, crowding can stabilize (by the ESM) or destabilize (depending on the quality of the solvent) proteins or be neutral. In other words, there are multiple possibilities and not a single universal scenario to capture the effects of crowding on protein or RNA stability. Only by studying the phase diagram over a wide range of conditions, rather than at a single external condition, can we hope to describe in quantitative detail the fate of a protein or RNA in the complex cellular environment.

## AUTHOR INFORMATION

### Corresponding Author

*E-mail: thirum@umd.edu.

### Notes

The authors declare no competing financial interest.

## ACKNOWLEDGMENTS

We are grateful to the National Science Foundation (CHE09-10433) for supporting this work.

## REFERENCES

(1) Elcock, A. *Curr. Opin. Strut. Biol.* **2010**, *20*, 196−206.
(2) Zhou, H. X.; Rivas, G.; Minton, A. P. *Ann. Rev. Biophys.* **2008**, *37*, 375−397.
(3) Dhar, A.; Samiotakis, A.; Ebbinghaus, S.; Nienhaus, L.; Homouz, D.; Gruebele, M.; Cheung, M. *Proc. Natl. Acad. Sci. U.S.A.* **2010**, *107*, 17586−17591.
(4) Cheung, M. S.; Klimov, D.; Thirumalai, D. *Proc. Natl. Acad. Sci. U.S.A.* **2005**, *102*, 4753−4758.

(5) Homouz, D.; Perham, M.; Samiotakis, A.; Cheung, M. S.; Wittung-Stafshede, P. *Proc. Natl. Acad. Sci. U.S.A.* **2008**, *105*, 11759−18981.
(6) Minton, A. *Biophys. J.* **2000**, *78*, 101−109.
(7) Minton, A. *Biophys. J.* **2005**, *88*, 971−985.
(8) Pincus, D.; Hyeon, C.; Thirumalai, D. *J. Am. Chem. Soc.* **2008**, *130*, 7364−7372.
(9) Kilburn, D.; Roh, J. H.; Guo, L.; Briber, R. M.; Woodson, S. A. *J. Am. Chem. Soc.* **2010**, *132*, 8690−8696.
(10) Denesyuk, N. A.; Thirumalai, D. *J. Am. Chem. Soc.* **2011**, *133*, 11858−11861.
(11) Sasahara, K.; McPhie, P.; Minton, A. *J. Mol. Biol.* **2003**, *326*, 1227−1237.
(12) McPhie, P.; Ni, Y.-s.; Minton, A. P. *J. Mol. Biol.* **2006**, *361*, 7−10.
(13) Waegele, M. M.; Gai, F. *J. Chem. Phys.* **2011**, 095104.
(14) Zimmerman, S. B.; Minton, A. P. *Annu. Rev. Biophys. Biomol. Struct.* **1993**, *22*, 27−75.
(15) Klimov, D.; Newfield, D.; Thirumalai, D. *Proc. Natl. Acad. Sci.* **2002**, *99*, 8019−8024.
(16) Stagg, L.; Zhang, S. Q.; Cheung, M. S.; Wittung-Stafshede, P. *Proc. Natl. Acad. Sci. U.S.A.* **2007**, *104*, 18976−18981.
(17) Wang, Q.; Cheung, M. S. *Biophys. J.* **2012**, *102*, 2353−2361.
(18) McGuffee, S. R.; Elcock, A. H. *PLoS Comput. Biol.* **2010**, *6*, e1000694.
(19) O'Brien, E. P.; Straub, J. E.; Brooks, B. R.; Thirumalai, D. *J. Phys. Chem. Lett.* **2011**, *2*, 1171−1177.
(20) Winzor, D.; Wills, P. *Biophys. Chem.* **2006**, *119*, 186−195.
(21) Minton, A. *Mol. Cell. Biochem.* **1983**, *55*, 119−140.
(22) Kudlay, A.; Cheung, M. S.; Thirumalai, D. *Phys. Rev. Lett.* **2009**, 102.
(23) Fleer, G. J.; Tuinier, R. *Adv. Colloid Interface Sci.* **2008**, *143*, 1−47.
(24) Hyeon, C.; Thirumalai, D. *Nat. Commun.* **2011**, *2*, 487.
(25) Case, D.; Cheatham, T.; Darden, T.; Gohlke, H.; Luo, R.; Merz, K.; Onufriev, A.; Simmerling, C.; Wang, B.; Woods, R. *J. Comput. Chem.* **2005**, *26*, 1668−1688.
(26) Guo, Z.; Thirumalai, D. *J. Mol. Biol.* **1996**, *263*, 323−343.
(27) Klimov, D. K.; Betancourt, M. R.; Thirumalai, D. *Folding Des.* **1998**, *3*, 481−498.
(28) Honeycutt, J. D.; Thirumalai, D. *Biopolymers* **1992**, *32*, 695−709.
(29) Chodera, J. D.; Swope, W. C.; Pitera, J. W.; Seok, C.; Dill, K. A. *J. Chem. Theory Comput.* **2007**, *3*, 26−41.
(30) Koutsioubas, A.; Lairez, D.; Combet, S.; Fadda, G. C.; Longeville, S.; Zalczer, G. *arxiv.org* **2011**, *1112*, 4676v.
(31) Asakura, S.; Oosawa, F. *J. Chem. Phys.* **1954**, *22*, 1255−1256.
(32) Shaw, M. R.; Thirumalai, D. *Phys. Rev. A* **1991**, *44*, 4797−4800.
(33) Thirumalai, D. *Phys. Rev. A.* **1988**, *37*, 269−276.
(34) Edwards, S.; Muthukumar, M. *J. Chem. Phys.* **1988**, *89*, 2435−2441.
(35) Honeycutt, J.; Thirumalai, D. *J. Chem. Phys.* **1989**, *90*, 4542−4559.
(36) van der Schoot, P. *Macromolecules* **1998**, *31*, 4635−4638.
(37) Kim, Y. C.; Best, R. B.; Mittal, J. *J. Chem. Phys.* **2010**, 133.
(38) Cotter, M. *Phys. Rev. A.* **1974**, *10*, 625−636.
(39) Brochard, F.; de Gennes, P. G. *Ferroelectrics* **1980**, *30*, 33−47.